PHYSICAL REVIEW E **75**, 020302(R) (2007)

Rapid two-dimensional imaging of bubbles and slugs in a three-dimensional, gas-solid, two-phase flow system using ultrafast magnetic resonance

C. R. Müller, D. J. Holland, J. F. Davidson, J. S. Dennis, L. F. Gladden, A. N. Hayhurst, M. D. Mantle, and A. J. Sederman
Department of Chemical Engineering, University of Cambridge, Pembroke Street, Cambridge CB2 3RA, United Kingdom
(Received 11 October 2006; published 9 February 2007)

Ultrafast magnetic resonance has been applied to measure the geometry of bubbles and slugs in a three-dimensional gas-solid two-phase flow. A bed of particles of diameter 0.5 mm were fluidized with gas velocities in the range of 0.08–0.26 m/s. Bubbles were imaged in transverse as well as vertical planes with an acquisition time of down to 25 ms and a spatial resolution down to 1.7 mm. Owing to the ultrafast character of these measurements, it is not only possible to evaluate correlations, e.g., for the bubble diameter, but also evaluate models of complex hydrodynamic phenomena, such as the splitting and coalescence of bubbles.

DOI: 10.1103/PhysRevE.75.020302 PACS number(s): 45.70.−n, 47.55.Kf, 47.55.Lm, 83.85.Fg

Owing to its complex behavior, granular matter has attracted considerable interest among engineers and more recently physicists [1]. The phenomena studied have included mixing and segregation in rotating drums [2] and vibrating beds [3,4], the dynamics of granular arrays flowing down an inclined plane [5,6], and partially and fully fluidized systems [7–10]. However, it is very challenging to image three-dimensional (3D) granular systems, as they are usually optically opaque. This limits the ability to observe phenomena such as axial segregation or the formation and coalescence of bubbles. Many experimental studies have been limited to two-dimensional (2D) systems [11,12], which are observable by optical measurement techniques, employing high-speed cameras. Experimental techniques do exist to make measurements in 3D, optically opaque systems; these include electrical capacitance tomography [13], x-ray tomography [14], positron emission particle tracking (PEPT) [15], and magnetic resonance (MR) [9,10,16–19]. The advantage of MR over these other techniques is that it can image the distribution of solids as well as their velocities in both single- and two-phase granular systems. MR is also chemically specific and therefore can track changes in composition, i.e., chemical reactions.

To date MR has mainly been applied to liquid phase systems, owing to the favorable relaxation properties of liquids. Imaging of granular systems is significantly more difficult because of the magnetic inhomogeneity and short nuclear spin-spin relaxation time constants characteristics of solid systems. Early investigations applying MR to granular systems have focused on imaging the solid phase and have included systems in which the system was stopped during acquisition, e.g., to measure the segregation of solids in rotating drums [20]. Alternatively, simple periodic systems, such as vibrating beds, were studied by averaging the signal at a certain point in the cycle over several cycles [21]. The first studies of gas-solids systems concentrated on gas-fluidized beds and have been reported only very recently [10,16–19]. A fluidized bed typically comprises a bed of granular solids supported on a porous plate in a vertical column, through which gas flows upwards. The solids become fluidized when the flow rate of gas is enough for the pressure drop across the bed to become equal to its weight per unit area of the column. The minimum superficial velocity of the gas required to fluidize the bed is U_{mf}. For particles in Geldart's group B or D, gas in excess of this minimum fluidization velocity forms bubbles. The dynamics of fluidized beds are inherently complex and involve very short time scales. However, most MR studies [10,17,18] report time-averaged measurements, such as particle velocities or time-averaged density profiles. Only two studies [16,19] report ultrafast 1D profiles; the measurements were, however, spatially averaged over a transverse plane, i.e., a plane orthogonal to the axis of the column. In the context of these studies, "ultrafast" refers to data acquisitions over time scales of 1–100 ms, which is fast relative to the second or minute time scales typical of standard MR pulse sequences. Acquisitions of such high time resolution enable imaging of dynamic processes in gas-solid flows, which evolve over these short time scales. In particular, Müller *et al.* [19] investigated the hydrodynamics in gas-fluidized beds using ultrafast MR. As the measurements were spatially averaged over a transverse plane, only the height and velocity of a bubble or slug could be determined. Direct imaging of the gas phase of a fluidized bed is less well-studied. However, a study of gas exchange between the bubble and emulsion phase as well as the velocity distribution of the gas, using hyperpolarized ^{129}Xe as the fluidizing gas, has been reported [9].

This Rapid Communication reports ultrafast, slice-selective MR of the integrated signal intensity associated with the solid phase in a horizontal plane of a gas-fluidized bed, giving 1D intensity profiles in a horizontal plane. Furthermore, 2D images both in transverse and vertical planes were acquired. These images enabled the direct observation of the 2D geometry of a bubble or slug in a 3D gas-fluidized bed. The images were obtained with spatial resolution and acquisition time such that the dynamics of individual bubbles coalescing could be observed in 2D. Finally, the effect of bubble motion during acquisition on the quantification of the measurements was studied (images shown in this Rapid Communication are zero-filled to a size of 64×64).

The fluidized bed was made of an acrylic column, i.d. (D_t) 50 mm, length 1.4 m. The distributor consisted of a drilled plate containing 37 holes, each 1.0 mm diameter. Seeds (Nudicaule; 500 μm mean diameter; Geldart B) were used as solids with U_{mf}=0.13 m/s. The height of the unfluidized bed, H_0, was either 355 or 255 mm. The bed was fluidized at

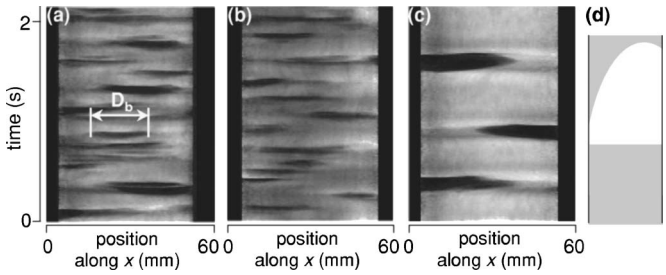

FIG. 1. Bubbles and slugs in a bed of H_0=255 mm: (a) Bubbles at h=45 mm, $U-U_{mf}$=0.13 m/s, (b) bubbles at h=75 mm, $U-U_{mf}$=0.08 m/s, (c) wall slugs at h=245 mm, $U-U_{mf}$=0.08 m/s, and (d) vertical cross section of an ideal wall slug.

U/U_{mf}=1.25–3.0, i.e., the excess gas velocities ranged between $U-U_{mf}$=0.03 and 0.26 m/s. The high oil content of the seeds enabled MR imaging. The fluidized bed was placed vertically in a Bruker DMX 200 spectrometer operating at a proton (^{1}H) frequency of 199.7 MHz. A birdcage radio frequency (rf) coil (i.d. 64 mm) positioned around the outside of the fluidized bed was used to excite and detect the MR signal from the seeds. Spatial resolution was achieved using a three-axis shielded gradient system capable of producing a maximum magnetic field gradient of 0.139 T/m. No signal was obtained from the fluidizing gas. To image bubbles and slugs in a 3D fluidized bed the following fast low-angle shot (FLASH) [22] pulse sequences were applied.

(i) Soft-pulse 1D FLASH. Here, a single horizontal slice was excited and thus a single voxel in one 1D profile represents the intensity averaged along the x or y axis, i.e., $I(x)=\int I(x,y)dy$ or $I(y)=\int I(x,y)dx$ at a given z position. In this Rapid Communication, the axis of the column is referred to as the z axis, whereas the x and y axes lie in a plane orthogonal to the axis of the column. The maximum bubble diameter can be derived from such measurements. The acquisition time was 4.4 ms and the spatial resolution along the line of sight was 469 μm. The slice thickness in the z-direction was 2.5 mm.

(ii) Soft-pulse 2D FLASH. A horizontal or vertical slice of the bed was excited and a full 2D intensity profile of the excited slice was then acquired. Depending on the spatial resolution, the acquisition resolution was either 25 or 50 ms. The spatial resolution of a horizontal slice was, respectively, 1.7×3.4 mm^2 and 0.9×1.7 mm^2 for the long and short values of the acquisition time. The corresponding spatial resolution of a vertical slice was, respectively, 1.7×4.1 mm^2 and 0.9×2.0 mm^2 for the long and short acquisition time. The slice thickness was 5.0 mm; for a vertical slice the phase encoding was in the axial direction.

FLASH images are reported, taken at heights 45, 75, 90, 150, and 245 mm above the distributor. At an axial height of 245 mm, the bed was in the slugging regime. Here, a slug is a bubble, whose diameter is close to the diameter of the column. Depending on particle size, bed diameter, and operating conditions, different types of slugs, i.e., wall-, axisymmetric, and flat-nosed slugs, can occur [23]. Below 150 mm, depending on the fluidization velocity, slugging or bubbling will prevail. Figure 1 shows slice selective 1D FLASH measurements.

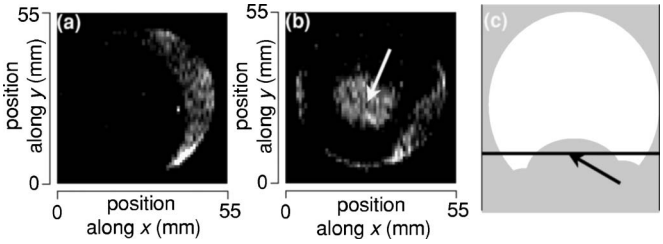

FIG. 2. (a) Wall slug at h=200 mm, $U-U_{mf}$=0.163 m/s, H_0=355 mm and (b) wake of a large bubble at h=70 mm, $U-U_{mf}$=0.163 m/s, H_0=355 mm. The arrow indicates the wake of the bubble. (c) Vertical cross section of a bubble attached to the wall. The black arrow indicates the wake of the bubble; the black horizontal line is the position at which the transverse slice (b) was taken.

Figures 1(a) and 1(b) give MR measurements at conditions where bubbling prevails. The maximum diameter of the bubble, D_b, can be extracted as shown in Fig. 1(a). In Fig. 1(a) at given values of radial position, y, and t, the shade of gray represents $\int_{-x_w}^{+x_w} I dx$, where x_w is the half-width of the column at a given y: white indicates densely packed particles; black implies no particles. Thus when a bubble is intersected, its size in y can be measured. As shown in Fig. 1(a), the y-dimension of the bubble increases with t and then decreases. The maximum value of this y-dimension gives the bubble diameter, D_b, assuming it is circular as seen from above. This estimate of D_b is irrespective of whether or not the bubble is central because the plot of $\int I dx$ against y includes the whole cross section. In Fig. 1(c), wall slugs are observed. These are bubbles of an equivalent spherical diameter $>0.6D_t$, attached to the wall, as shown schematically in Fig. 1(d). It was observed visually that wall slugs occurred at small excess gas velocities high up the bed, just before the slugs erupted. An interesting feature in Fig. 1(c) is the fact that the side on which the slug is attached to the wall seems to oscillate quite regularly (based on longer observation times, not shown here). The frequency of the passing wall slugs, shown in Fig. 1(c) is ~2 Hz.

Selected 2D FLASH images of a horizontal slice are

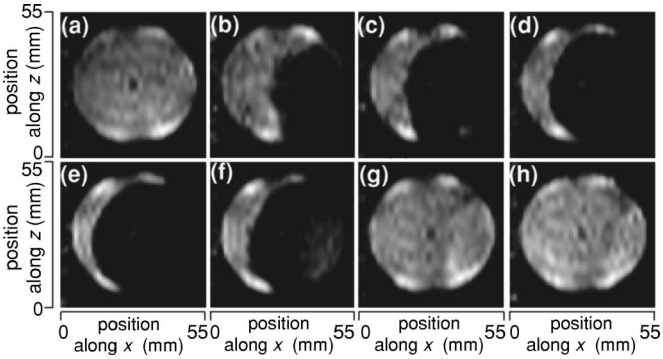

FIG. 3. Series of images showing a slug passing through a horizontal slice. $U-U_{mf}$=0.136 m/s, h=250 mm, H_0=355 mm. The time sequence is (a),(b),…,(h) and the time interval between images is 25 ms. Thus a total time of 375 ms is covered by the images (a)–(h).

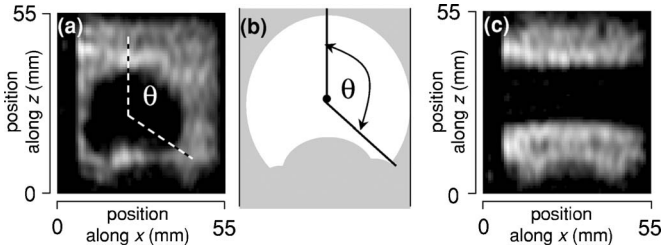

FIG. 4. (a) Large bubble $h=90$ mm, $U-U_{mf}=0.13$ m/s, $H_0=355$ mm, (b) definition of the wake angle, and (c) flat-nosed slug at $h=90$ mm, $U-U_{mf}=0.13$ m/s, $H_0=355$ mm.

shown in Fig. 2. Figure 2(a) gives the horizontal profile of a wall slug, similar to the one shown in Fig. 1(d). A particularly interesting feature of these two 2D measurements is the wake of a bubble, given in Fig. 2(b). A vertical sketch of the bubble in Fig. 2(b) is given in Fig. 2(c). The horizontal line in Fig. 2(c) indicates the position where Fig. 2(b) was acquired. The wake-region of the bubble is indicated by an arrow, Figs. 2(b) and 2(c). Figures 2(a) and 2(b) provide direct visualization of bubble-wall interactions. It is worth noting that although only single images are displayed here, it was possible to acquire sequentially a series of up to 50 images at either 25 or 50 ms intervals. An example of part of such a series (8 images, 25 ms acquisition for one single image) is given in Fig. 3, where the progression of a bubble through the imaging slice can be observed. 2D FLASH data from a vertical slice are shown in Fig. 4. The slice thickness for the vertical slice was 5.0 mm and the phase encoding was in the axial direction. Figure 4(a) shows the shape of a typical bubble where the wake of the bubble can again clearly be observed. A wake angle of $\theta\sim 135°$ can be extracted from Fig. 4(a), typical for bubbles in the system studied [23]. Figure 4(c) shows a so-called flat-nosed slug, often observed in columns of small diameters, as used here.

Darton *et al.* [24] developed an equation for predicting the bubble diameter based on a bubble coalescence model. The model contains one empirical constant for the distance between two coalescence events, derived from observing the eruption of two bubbles, which have been successively injected into fluidized beds [25]. The equivalent spherical bubble diameter is predicted [24] as $D_b=0.54(U-U_{mf})^{0.8}(h+4\sqrt{A_0})^{0.4}/g^{0.2}$, where $U-U_{mf}$, h, and A_0 are the excess gas velocity, height above the distributor, and area per hole at the distributor, respectively. For an excess gas velocity of $U-U_{mf}=0.13$ m/s the equivalent bubble diameter at a height $h=90$ mm is therefore $D_b=28.6$ mm ($A_0=0.53\times 10^{-4}$ m^2). The equivalent bubble diameter measured from 2D vertical FLASH data was 22±2 mm (the uncertainty quoted is the standard deviation based on measurements of 13 bubbles; it does not refer to the spatial resolution of the measurements). The calculation was based on the following assumptions: (i) the bubbles are axisymmetric and (ii) the vertical plane goes through the axis of symmetry of the bubble. Transverse 2D FLASH images indicate that unconfined bubbles are approximately axisymmetric (the ratio of minimum to maximum bubble diameters being 0.87) and therefore the first assumption is valid. The second assumption constrains the choice of bubbles from which the mean bubble diameter is calculated, to be only those rising near the axis of the bed. Bubbles attached to the wall, and flat-nosed slugs, were ignored in the calculation of the bubble diameter. Thus the experimentally determined mean bubble diameter can be regarded as a lower limit of the bubble diameter. It is important to consider the effect of bubble motion during the acquisition time. To evaluate this, a numerical simulation of a 2D FLASH sequence was performed. The assumption that the bubble moves only in the vertical (phase) direction was made. This assumption may not be true near the distributor, but at heights greater than $\sim D_t$ it is reasonable. For example, the shape of the bubbles shown in Figs. 1(a) and 1(b) confirm this assumption because the radial position of the bubble does not change significantly during its passage through a transverse plane. The simulation was performed in a similar manner to [26]. Binary images of gas-solid distributions were generated on a 256×256 grid which were then binned down to the acquisition array size of 64×32. A bubble speed of 0.2 m/s was assumed; typical of large bubbles, as shown in Fig. 4 [19]. Consequently, the bubble, modeled by a disk, moves five voxels during the acquisition of the image (acquisition time of 50 ms for the image). Taking the motion of

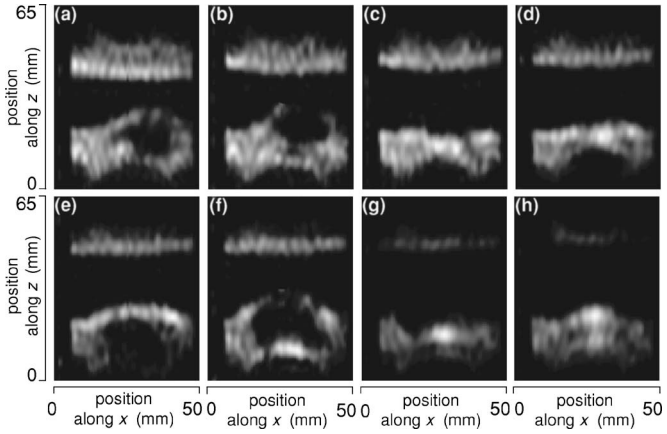

FIG. 5. Sequential coalescence of two small bubbles with a flat-nosed slug recorded over ~200 ms at $h=90$ mm, $U-U_{mf}=0.13$ m/s, $H_0=355$ mm.

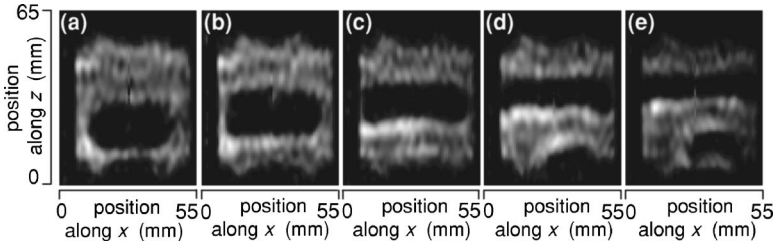

FIG. 6. Formation of a square-nosed slug, $h=90$ mm, $U-U_{mf}=0.13$ m/s. Total time for (a)–(e) is 125 ms, $H_0=355$ mm.

the bubble into account, time domain data were generated and then the image was reconstructed via Fourier transformation. Selecting the point in the simulated data at which the intensity is equal to 0.5 recovers the original image, i.e., the diameter of the bubble, to within the spatial resolution of the image in agreement with [26]. Finally, the capture of coalescence in 2D is reported. Figure 5 shows the consecutive coalescence of two small bubbles with a flat-nosed slug. Compared with bubbles, flat-nosed slugs rise slowly in a fluidized bed, and are thus ideal for observing bubble coalescence. In Figs. 5(a)–5(c) the first bubble merges from below with the flat-nosed slug. It can be seen that during coalescence, the thickness of the layer of particles separating the bubble and the slug decreases until the following bubble breaks through. The second coalescence event in Figs. 5(e)–5(h) is very similar, but here the wake of the trailing bubble is entrained more conspicuously than in the previous image into the flat-nosed slug, see, Fig. 5(h). Another interesting example of the capture of a hydrodynamic phenomenon, using ultrafast MR, is the formation of a flat-nosed slug from a bubble. This is seen in Fig. 6, which shows how, within 125 ms, a bubble expands horizontally until its diameter equals the column diameter. In this Rapid Communication rapid 2D MR measurements on a two-phase granular system are reported. The images are of sufficient quality to determine the dimensions of bubbles and slugs. Owing to the ultrafast acquisition sequence, the high resolution images of bubble coalescence in 3D granular systems are reported. Such measurements, in conjunction with 1D FLASH profiles [19], will enable the determination of the velocity and geometry of bubbles in 3D systems. Furthermore, a critical evaluation of existing bubble coalescence models in 3D systems is now possible.

One of the authors (C.R.M.) wishes to acknowledge both the Deutscher Akademischer Austauschdienst (DAAD) and the Cambridge European Trust for financial support. L.F.G., J.S.D., D.J.H., A.J.S., and M.D.M. acknowledge financial support from the EPSRC (EP/C 547195/1 and GR/S20789/01).

[1] H. M. Jaeger *et al.*, Rev. Mod. Phys. **68**, 1259 (1969).
[2] K. M. Hill, A. Caprihan, and J. Kakalios, Phys. Rev. Lett. **78**, 50 (1997).
[3] P. Evesque and J. Rajchenbach, Phys. Rev. Lett. **62**, 44 (1989).
[4] E. E. Ehrichs *et al.*, Science **267**, 1632 (1995).
[5] L. E. Silbert, Phys. Rev. Lett. **94**, 098002 (2005).
[6] O. Pouliquen, Phys. Rev. Lett. **93**, 248001 (2004).
[7] D. Volfson, L. S. Tsimring, and I. S. Aranson, Phys. Rev. Lett. **90**, 254301 (2003).
[8] C. Huan, X. Yang, D. Candela, R. W. Mair, and R. L. Walsworth, Phys. Rev. E **69**, 041302 (2004).
[9] R. Wang *et al.*, Magn. Reson. Imaging **23**, 203 (2005).
[10] R. Savelsberg, D. E. Demco, B. Blumich, and S. Staph, Phys. Rev. E **65**, 020301(R) (2002).
[11] S. P. Sit and J. R. Grace, Chem. Eng. Sci. **36**, 327 (1981).
[12] P. Pandey *et al.*, Powder Technol. **161**, 79 (2006).
[13] Y. T. Makkawi and P. C. Wright, Chem. Eng. Sci. **57**, 2411 (2002).
[14] P. N. Rowe and C. X. R. Yocono, Chem. Eng. Sci. **31**, 1179 (1976).
[15] R. D. Wildman and D. J. Parker, Phys. Rev. Lett. **88**, 064301 (2002).
[16] P. S. Fennell *et al.*, Chem. Eng. Sci. **60**, 2085 (2005).
[17] S. Harms, S. Stapf, and B. Blümich, J. Magn. Reson. **178**, 308 (2006).
[18] A. C. Rees *et al.*, Chem. Eng. Sci. **61**, 6002 (2006).
[19] C. R. Müller *et al.*, Phys. Rev. Lett. **96**, 154504 (2006).
[20] S. L. Conway, T. Shinbrot, and B. J. Glasser, Nature (London) **431**, 433 (2004).
[21] J. M. Huntley *et al.*, *Proceedings of the 5th World Congress on Particle Technology, Orlando, 2006*.
[22] A. Haase *et al.*, J. Magn. Reson. (1969-1992) **67**, 194 (1986).
[23] D. Kunii and O. Levenspiel, *Fluidization Engineering* (Butterworth-Heinemann, Stoneham, 1991).
[24] R. C. Darton *et al.*, Trans. Inst. Chem. Eng. **55**, 274 (1977).
[25] D. Harrison and L. S. Leung, *Symposium on the Interaction Between Fluids and Solids*, edited by P. A. Rottenburg (Institution of Chemical Engineers, London, 1962), p. 127.
[26] A. J. Sederman, M. D. Mantle and L. F. Gladden, J. Magn. Reson. **161**, 15 (2003).